Sixfold ring clustering in sp^2-dominated carbon and carbon nitride thin films: A Raman spectroscopy study

G. Abrasonis*
Institute of Ion Beam Physics and Materials Research, Forschungszentrum Rossendorf, PF-510119, 01314 Dresden, Germany

R. Gago
Centro de Micro-Análisis de Materiales y Departamento de Física Aplicada, Universidad Autónoma de Madrid, E-28049 Cantoblanco, Madrid, Spain

M. Vinnichenko, U. Kreissig, A. Kolitsch, and W. Möller
Institute of Ion Beam Physics and Materials Research, Forschungszentrum Rossendorf, PF-510119, 01314 Dresden, Germany
(Received 26 October 2005; revised manuscript received 17 January 2006; published 24 March 2006)

The atomic arrangement in sp^2-dominated carbon (C) and carbon nitride (CN_x) thin films has been studied by Raman spectroscopy as a function of substrate temperature and, in the case of CN_x, different N incorporation routes (growth methods). In this way, materials composing graphitelike, fullerenelike (FL), and paracyanogenlike structures have been compared. The results show that each type of arrangement results in a characteristic set of the Raman spectra parameters, which describe the degree of aromatic clustering, bond length, and angle distortion and order in sixfold structures. In the case of C films, the atomic structure evolves with substrate temperature from a disordered network to nanocrystalline planar graphitic configurations, with a progressive promotion in size and ordering of sixfold ring clusters. Nitrogen incorporation favors the promotion of sixfold rings in highly disordered networks produced at low temperatures, but precludes the formation of extended graphiticlike clusters at elevated substrate temperatures (>700 K). In the latter case, N introduces a high degree of disorder in sixfold ring clusters and enhances the formation of a FL microstructure. The formation and growth of aromatic clusters are discussed in terms of substrate temperature, N incorporation, growth rate, film-forming sources, and concurrent bombardment by hyperthermal particles during growth.

DOI: 10.1103/PhysRevB.73.125427 PACS number(s): 78.30.Na, 78.30.Ly, 63.50.+x, 81.15.Cd

INTRODUCTION

Carbon nitrides (CN_x) represent an important class of materials due to their large variety in microstructure, which results in a wide range of mechanical,[1] electrical,[2–6] and optical[2,7–10] properties. The variety of CN_x structures is mainly due to the capability of both elements, carbon and nitrogen, to adopt different possible states of hybridization (sp^1, sp^2, and sp^3). Although the research in CN_x solids has been mainly driven by the search of novel superhard materials with sp^3 structures (for example, the β-C_3N_4 phase proposed by Liu and Cohen[11]), most of the attempts resulted in sp^2-dominated materials. Despite these results, the sp^2-dominated materials have shown very interesting properties. The most promising materials are referred to as fullerenelike (FL) CN_x, owing the notation to their microstructure composed of a 3D arrangement of extended, bent, and cross-linked N-containing graphitic basal planes.[12] Fullerenelike CN_x exhibits large hardness with extremely large elastic recovery.[1,12–14] On the other hand, some modifications of sp^2-dominated CN_x exhibit diamondlike electrical resistivity and thermal conductivity combined with high thermal stability.[15]

Nitrogen plays an important role in the formation and dominance of a particular local bonding environment. This is due to the capability of N to accommodate different local atomic arrangements such as substituting C in aromatic clusters or terminating pyridinelike or nitrilelike configurations.[16,17] The latter hinder the growth of aromatic clusters,[18] while the former promote the extension of the graphene sheets,[19] the formation of pentagons, which induce the curvature in the basal planes,[12,20] and cross-linking between adjacent planes.[12,21,22] Besides, the capability of N to influence the cluster size and order may control the localization of the electrons [extension of the orbitals, electron (hole) mobility], while N incorporation into certain configurations induces doping.[20] The proportion and arrangement of these competing local bonding structures depend on the N incorporation routes into a C network, which is determined by the synthesis technique and treatment conditions.

Apart from the information about local bonding environments, medium-range ordering features are relevant to understand the final film properties. In particular, sp^2 arrangements will define the electronical properties of the material.[16,23] In general, sp^2-dominated CN_x networks exhibit different proportions of chain and aromatic structures and different degrees of extension, bending, and cross-linking of aromatic clusters. Raman spectroscopy is a powerful and nondestructive technique that provides quantitative information about the medium-range ordering, which comprises the degree of aromatic clustering, the bond angle distortion, and the ordering inside graphene planes.[16,17,23–27] This renders this technique a powerful tool for characterization of different modifications of C and CN_x. The purpose of this study is to quantitatively estimate the degree and properties of sixfold ring clustering in sp^2-dominated C and CN_x thin films as a function of the growth conditions. For this, C and CN_x films grown using different growth methods, each of them involv-

ing different C and N sources, will be compared. The use of different growth methods aims at the formation of graphitelike, paracyanogenlike, and fullerenelike sp^2 arrangements. It will be shown that Raman spectra exhibit characteristic features for each type of sp^2 arrangement, describing the characteristic bond strength and angle distortion, the degree of aromatic clustering, and the ordering inside the clusters. From this, information about local atomic bond configurations can be derived. The double role of N, inducing/enhancing sp^2 order at lower temperatures ($<\sim 150\ ^\circ C$), and creating disorder at higher temperatures ($>\sim 150\ ^\circ C$), will be demonstrated. The influence of different C and N incorporation routes, ion bombardment, and film growth rate on the ordering, clustering, and curvature of the aromatic clusters will be discussed.

EXPERIMENT

Thin film growth

Carbon and carbon nitride films have been grown by ion beam sputtering (IBS), dual ion beam deposition (DIBD), ion beam assisted evaporation (IBAE), and dc-magnetron sputtering (MS). The main differences between each of the growth methods are basically the energy distribution of the film-forming species, the presence of concurrent ion bombardment during growth, and the participation of atomic or polyatomic species. In IBS, DIBD, and MS, the main C source is the sputtered flux from a graphite target, which carries higher energy (up to a few ten eV) than in the case of evaporation (in the range of 0.1 eV).[28,29] Simultaneously, the growing film surface is bombarded by ions reflected from the target, with energies of several hundreds of eV.[30] During sputtering using a N_2/Ar mixture in IBS, DIBD, and MS, N is delivered by sputtered N and CN particles from the previously nitride target (few eV).[31,32] Finally, in the case of IBAE, the source of N is $\sim$60 eV N_2^+ and N^+ ions from the assisting ion gun. The ion bombardment is also present in DIBD ($\sim$100 eV) and MS (25–40 eV), implying an additional source of N for assistance.

The details of each deposition method and working conditions have been reported elsewhere for IBS,[31] DIBD,[31] IBAE,[18] and MS.[33] The dominance of sp^2 hybrids in all as-grown samples was confirmed by x-ray near-edge absorption spectroscopy (XANES).[18,19,31] Regarding the network arrangements, IBAE films present a large amount of nitrilelike environments and, therefore, impose a low-density amorphous structure with a paracyanogenlike character.[18] MS deposition leads to the formation of a pronounced FL microstructure[33] where the majority of N is inserted inside the graphene sheets in threefold graphitelike sites.[19] IBS and DIBD yield arrangements in between graphitelike and FL.[34] Film composition, areal density, and incorporation rate were obtained from elastic recoil detection analysis (ERDA) (for details, see Ref. 18), while the mass densities were derived from a combination with thickness measurements by spectroscopic ellipsometry (for details, see Refs. 18 and 35). The film growth conditions, compositions, areal densities, incorporation rates, and mass densities are summarized in Table I.

Visible Raman spectroscopy analysis

The bonding structure of the deposited films was characterized using Raman spectroscopy. Micro-Raman spectra were collected with a LABRAM HR 800 microspectrometer at an excitation wavelength of 532 nm (2.3 eV). This energy resonates with π-π^* electronic transitions in ring structures,[23] which makes it suitable for the study of aromatic clustering processes in sp^2-dominated solids. The power density on the sample was below 0.4 MW m^{-2} to avoid unintentional modification of the bonding structure of the samples (confirmed by repetitive measurements on the same sample position). The spectral resolution achieved with the system is 1 cm^{-1}, and the spectral slit width is 4 cm^{-1}.

FITTING PROCEDURE OF THE RAMAN SPECTRA

Raman spectra of C and CN_x films in the wave-number region of 900–2000 cm^{-1} exhibit usually two main peaks positioned at $\sim$1350 and $\sim$1560–1590 cm^{-1} which are denoted conventionally by D and G, respectively. The G ("graphite") peak is due to in-plane bond stretching vibrations. This mode is a single resonance and can be present in aromatic clusters as well as in chain structures.[23] The D ("disorder") mode is a double resonance[36] and is associated with breathing vibrations of aromatic rings. It can be present only in ring structures. The D peak is not present in the single crystalline graphite spectra or in completely amorphous C films. The intensity of this peak is due to two concurrent factors:[23] (i) relaxation of the $k\approx 0$ rule when the size of the graphitic grains decreases, from which modes being far away from the center of the Brillouin zone can be observed; (ii) the presence of ring structure.

When N is introduced into a C network, the CN vibration frequencies for chainlike molecules and ringlike molecules are very close to those of pure C.[16] The modes are delocalized over both C and N sites due to the capability of N to acquire the same hybridizations as C atoms. Following this, the same approach as used for various C films can be applied to CN_x films. This is important for the present study case, because in some films N is present, while others are free from N.

All Raman spectra (both for C and CN_x) were fitted with the same type of fit functions. The combination of a linear background, a symmetric Lorentzian, and asymmetric Breit-Wigner-Fano (BWF) shape to fit the D and G peaks, respectively, was found to be a good compromise between the fitting quality and the capability to fit all spectra. The BWF line shape is described by the following expression:[23,26]

$$I(k) = \frac{I_0[1 + 2(k - k_0)/q\Gamma]^2}{1 + [2(k - k_0)/\Gamma]^2}, \tag{1}$$

with the maximum positioned at[23]

$$k_{\max} = k_0 + \Gamma/2q, \tag{2}$$

where $I(k)$ is the intensity as a function of wave number k, I_0 is the peak intensity, k_0, $k_{\max}$ and Γ are the mean peak position, the peak position at the maximum, and the full width at

TABLE I. Composition, areal density, incorporation rate, thickness and, mass density of the C and CN_x films grown by IBS, DIBD, MS, and IBAE at different temperatures, N_2 ratios, assisting ion currents, and energies. For IBS, the N_2 ratios correspond to the mass flow ratios in the sputtering beam, while for MS they correspond to N_2 ratios in the sputtering gas. ERDA data of IBS and DIBD films are taken from Ref. 31, while some ERDA data of IBAE films are taken from Ref. 18.

Deposition method	T (°C)	N_2 (%)	j_N (μA cm^{-2})	Ion energy eV	Atomic ratio C %	N %	O %	H %	Film areal density (10^{18} cm^{-2})	Incorporation rate (10^{15} cm^{-2} s^{-1})	Film thickness nm	Mass density (g cm^{-3})
IBS	RT	0			92	1	1	6	0.93	0.13	66	2.7
	RT	25			82	11	1	7	1.06	0.15	82	2.5
	RT	50			80	13	1	6	1.11	0.15	82	2.6
	RT	75			76	17	1	7	0.97	0.13	79	2.4
	RT	100			73	21	1	5	0.87	0.12	77	2.2
	150	0			96	1	1	2	0.94	0.13	78	2.2
	150	25			89	9	1	2	1.00	0.14	87	2.2
	150	50			85	13	1	2	0.98	0.14	84	2.3
	150	75			83	13	1	3	0.86	0.12	73	2.3
	150	100			79	18	1	3	0.81	0.11	70	2.3
	300	0			98	1	0	1	0.89	0.12	99	1.8
	300	25			89	10	0	1	0.93	0.13	96	2.0
	300	50			88	11	1	1	0.90	0.13	93	2.0
	300	75			82	16	1	1	0.74	0.10	74	2.0
	300	100			81	17	1	2	0.75	0.10	72	2.1
	450	0			98	1	0	1	0.83	0.12	99	1.7
	450	25			91	8	1	1	0.93	0.13	99	1.9
	450	50			90	9	1	1	0.89	0.12	91	2.0
	450	75			87	11	1	1	0.79	0.11	85	1.9
	450	100			84	14	1	1	0.68	0.09	63	2.2
DIBD	450	100	3.6	100	68	26	0	6	0.55	0.08		
MS	150	16		25	78	22	0	0	1.28	0.53	97	2.8
	300	16		25	79	21	0	0	1.40	0.58	148	2.0
	450	16		25	81	18	0	1	1.20	0.50	126	2.0
	450	50		25	81	18	0	1	1.38	0.58	130	2.2
	450	100		25	84	16	0	0	1.33	0.55	118	2.3
IBAE	RT		0	60	82	0	5	13	0.99	1.65	74	2.4
	300		40	60	77	14	2	7	0.57	0.95	45	2.5
	300		71	60	72	16	3	9	0.29	0.48	36	1.5
	300		93	60	68	16	5	11	0.17	0.28	31	1.0
	RT		71	60	70	24	2	5	0.28	0.95	49	1.2
	300		71	60	70	23	3	5	0.25	0.83	39	1.3
	400		71	60	69	22	4	6	0.23	0.75	36	1.3
	480		71	60	67	25	2	5	0.21	0.70	34	1.3

half maximum, respectively, and q is the BWF coupling coefficient. In the following, the position of the G peak will be defined by $k_{\max}$. In the limit $q \to 0$, the Lorentzian line shape is reproduced. In implantation and annealing studies of graphite and glassy carbon,[24,26,37] it was established that in the limit $\Gamma_G/q \to 0$, the in-plane graphene ordering is complete, and three-dimensional ordering begins. Following this, Γ_G/q will be used to quantify the in-plane graphitic order.

As was mentioned above, the G peak is related to the vibrations present in the sp^2 phase, both in the olefinic and ring structures, while the D mode is related to the vibrations of the sixfold rings. When the Lorentz-BWF combination is used to fit the D and G peaks, the intensity ratio of D and G peaks I_D/I_G is related to the aromatic cluster size L_a.[23] However, the intensity of the D peak is due to two competing mechanisms (see above): the disorder-induced relaxation of the $k \approx 0$ rule (Tuinstra-Koenig effect)[38] and the probability to find an aromatic ring in the sp^2 phase. Following the three-stage model proposed by Ferrari *et al.*,[23] the reduction of the grain size in the perfectly oriented graphite will induce the appearance of the D peak, whose intensity will increase

as the grain size decreases. In this regime, the Tuinstra-Koenig relation is valid,[38]

$$L_a = 44 \times (I_D/I_G)^{-1} \text{ Å} \quad (3)$$

for the excitation laser wavelength of 514.5 nm. This expression is valid down to a critical cluster size of 20 Å,[23] below which the second mechanism starts to act. Then, the I_D/I_G ratio decreases with decreasing cluster size L_a according to Ref. 23,

$$L_a = [(I_D/I_G)/0.0055]^{1/2} \text{ Å}. \quad (4)$$

In this regime, the aromatic clusters become smaller and more disordered. When the disorder increases, the sp^2 phase changes from ring to chain structures, while at the final stage when sp^3 bonds are introduced the sp^2 bonds become strongly localized.

The fitting of the Raman spectra of the IBS samples grown at room temperature (RT) requires special comments. Due to the low intensity of the *D* peak (see below), fitting of the Raman spectra yield *D* peak position values almost coinciding with those of the *G* peak. Due to this, for each Raman spectrum of these films fitting was performed for several fixed *D* peak positions (in the range of 1365–1385 cm^{-1}), and then averaging the fitted parameters over all fits. As the intensity of the *D* peaks is very low, this does not influence the parameters of the *G* peak significantly.

In some CN_x films, another low intensity peak could be observed at ~2250 cm^{-1} related to the vibrations of sp^1 bonded C≡N groups.[16–18,39] However, the Raman excitation energy used in this study is too low to resonate with the π-π^* transitions of these groups,[16] thus the intensities obtained from the spectral fitting cannot be compared to those of the *G* and *D* vibrations where this energy causes the π-π^* electronic transitions. Instead, the contribution of these groups was investigated using XANES as presented elsewhere.[18,19,31] Consequently, the analysis of the Raman spectral features at ~2250 cm^{-1} will be omitted here.

EXPERIMENTAL RESULTS AND DISCUSSION

Raman spectra for carbon nitride films with different N content and growth temperature

Figures 1(a) and 1(b) present typical Raman spectra of the IBS films in the wave-number region of 900–2000 cm^{-1}. *D* and *G* peaks can be observed for the majority of the spectra, and for some of the spectra a small peak at ~960 cm^{-1} of the underlying Si substrate could also be seen. For the IBS films grown at RT, the *D* peak contribution is very low and can be hardly resolved in the spectra. Similar Raman spectra were also observed in amorphous carbon (*a*-C) films grown at RT by IBS (Ref. 25) and MS without additional bias.[40] Two main observations are the slight increase in the intensity of the *D* peak with N incorporation [Fig. 1(a)] and temperature [Fig. 1(a) and 1(b)]. The former indicates N-induced clustering of the sp^2 phase into ring structures, while the second points to a temperature-induced graphitization. All the spectra lack sharp features, except the C film grown at 450 °C. However, these sharp features of the *D* and *G* peaks are not present under the same growth conditions when N is incorporated, indicating increased disorder.

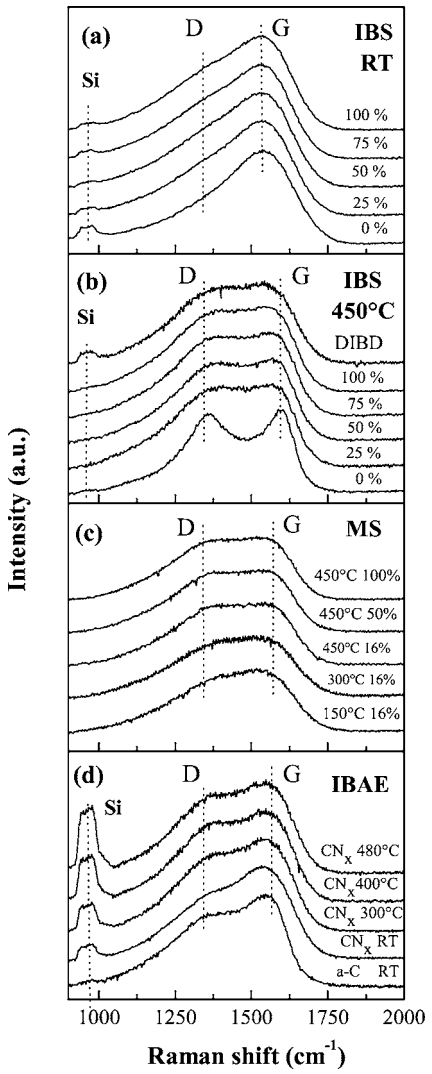

FIG. 1. Normalized Raman spectra of films grown by IBS, DIBD (a,b), MS (c), carbon evaporation, and IBAE (d). IBS CN_x films were grown at RT (a) and 450 °C (b) for different N_2 mass flow ratios. DIBD CN_x film was grown at 450 °C with pure N_2 sputtering and assisting beams (b). MS CN_x films were grown at different temperatures and N_2 ratios in the sputtering gas (c). Evaporated *a*-C film was grown at RT, while IBAE CN_x films were grown with assisting $N_2^+ + N^+$ ion current density of 71 μA cm^{-2} at RT, 300, 400, and 450 °C (d).

Raman spectra fitting results of the IBS samples are collected in Table II. For illustration, the fitting results of IBS grown films are presented in Fig. 2. From the dependence of the *G* peak positions and the *G* width Γ_G on the N atomic ratio of the films [Figs. 2(a) and 2(b), two different growth regimes can be identified: below and above ~150 °C. At RT, the position of the *G* peak slightly increases as the N atomic ratio in the film increases, while at higher temperatures it decreases. For a given N atomic ratio, the *G* peak shifts toward larger values when the temperature increases, and this shift is larger for lower N atomic ratios. Opposite trends can be seen for the dependence of the *G*peak width Γ_G. Gen-

TABLE II. Raman spectra fitting results of the C and CN_x films grown by IBS, DIBD, MS, and IBAE at different temperatures, N_2 ratios, assisting ion currents, and energies. For IBS and DIBD, N_2 ratios correspond to the mass flow ratios in the sputtering beam, while for MS they correspond to N_2 ratios in the sputtering gas.

					D peak		*G* peak					
Deposition method	T (°C)	N_2 (%)	j_N (μA cm^{-2})	Ion energy (eV)	Center (cm^{-1})	Γ_D (cm^{-1})	Center (cm^{-1})	Γ_G (cm^{-1})	q	$\lvert\Gamma_G/q\rvert$ (cm^{-1})	I_D/I_G	L_a (Å)
IBS	RT	0					1542	272	−3.14	86	0.08	3.8
	RT	25					1545	248	−3.01	83	0.33	7.7
	RT	50					1546	243	−2.91	84	0.42	8.8
	RT	75					1546	231	−2.91	79	0.48	9.4
	RT	100					1548	227	−2.78	82	0.61	10.5
	150	0			1369	183	1563	202	−2.57	79	0.83	12.3
	150	25			1381	217	1564	193	−2.15	90	1.17	14.6
	150	50			1377	212	1559	200	−2.26	88	1.09	14.1
	150	75			1371	204	1559	201	−2.40	84	1.01	13.6
	150	100			1376	218	1558	200	−2.36	85	1.07	14.0
	300	0			1360	164	1581	163	−2.75	59	0.99	13.4
	300	25			1370	205	1571	185	−2.19	84	1.25	15.1
	300	50			1368	202	1571	184	−2.29	80	1.18	14.7
	300	75			1368	202	1567	187	−2.36	79	1.18	14.7
	300	100			1366	201	1564	192	−2.41	80	1.12	14.3
	450	0			1358	98	1597	120	−3.62	33	0.90	48.9
	450	25			1370	189	1581	167	−2.31	72	1.21	14.9
	450	50			1368	179	1582	165	−2.55	65	1.14	14.4
	450	75			1366	184	1578	174	−2.46	71	1.14	14.4
	450	100			1368	198	1573	183	−2.29	80	1.20	14.8
DIBD	450	100	3.6	100	1364	194	1567	209	−2.47	85	1.13	14.3
MS	150	16		25	1393	236	1558	218	−2.09	104	1.33	15.6
	300	16		25	1383	230	1564	222	−2.13	104	1.38	15.8
	450	16		25	1373	194	1572	193	−2.35	82	1.25	15.1
	450	50		25	1368	194	1570	193	−2.45	79	1.22	14.9
	450	100		25	1362	200	1565	191	−2.38	81	1.26	15.2
IBAE	RT		0	60	1379	212	1553	199	−2.31	86	0.92	12.9
	300		40	60	1363	199	1567	180	−2.84	63	1.10	14.2
	300		71	60	1361	163	1564	194	−3.32	59	0.81	12.2
	300		93	60	1363	158	1564	192	−3.27	59	0.80	12.1
	RT		71	60	1356	184	1555	219	−3.35	65	0.58	10.3
	300		71	60	1362	170	1563	199	−3.16	63	0.80	12.1
	400		71	60	1364	161	1565	191	−3.08	62	0.87	12.6
	480		71	60	1358	166	1563	201	−2.98	67	0.83	12.3

erally, the *G* peak position reflects the bonding strength, and Γ_G reflects bond length and angle distortion.[16,25,26,41]

Additional information can be obtained by plotting the coupling parameter of the *G* peak Γ_G/q and the *D* peak width Γ_D versus the N atomic ratio for 150, 300, and 450 °C [Figs. 2(c) and 2(d)]. Both parameters exhibit very similar behavior, reflecting the changes in the ring structures. For pure C films, Γ_G/q approaches zero when the temperature increases, which means that graphene plane ordering increases and approaches the stage when three-dimensional ordering begins.[24] However, when some N is introduced into the films, it increases significantly the disorder in the ring structures, which is more pronounced for higher temperatures. Increasing the N atomic ratio above ~10 at. % does not induce any significant changes in both Γ_G/q and Γ_D. At the same time, for a given composition, Γ_G/q and Γ_D do not vary significantly with temperature, and this variation is lower for higher N atomic ratios. For the IBS films grown at RT, Γ_G/q is approximately equal to ~80–85 cm^{-1} and does not depend on the N content.

The evolution of the aromatic cluster size can be traced by plotting the cluster diameter L_a versus N atomic ratio for different temperatures [see Fig. 2(e)]. The question then arises which of the relations—Eq. (3) or Eq. (4)—should be

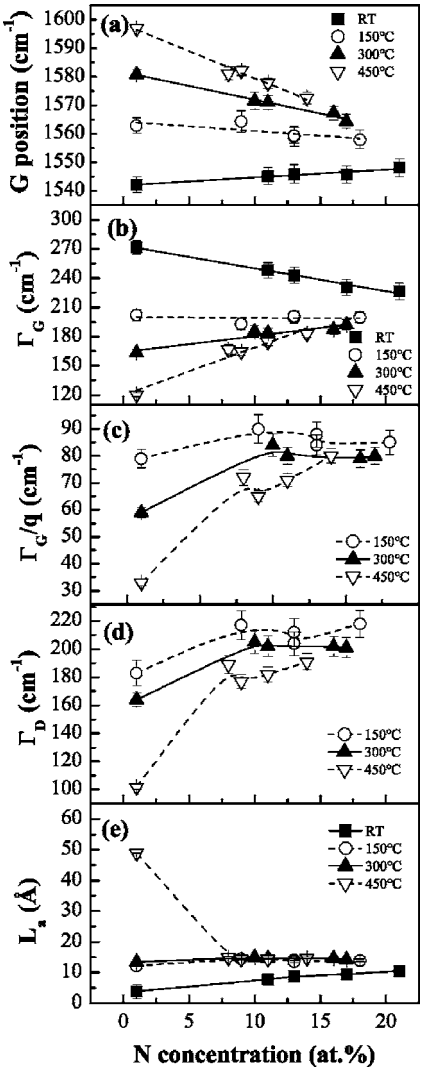

FIG. 2. Position (a), width Γ_G (b), and coupling parameter Γ_G/q (c) of the G peak, width Γ_D of the D peak (d), and cluster diameter L_a (e) vs N concentration for the C and CN_x films grown by IBS at different temperatures. In (a) and (b), lines represent linear fits, while in (c)–(e), lines are guiding the eye only. The error bars represent the 95% confidence limits of the fittings.

used to estimate L_a. The choice was made using the following arguments. For the samples prepared at RT, the intensity of the D peak is very low, so these samples should belong to the region of L_a where Eq. (4) is valid. As all other samples show similar Γ_G/q values [except pure C grown at ~450 °C—see Fig. 2(c)], it is expected that these samples also belong to the same L_a region where Eq. (4) can be used. For the C film produced at ~450 °C, the I_D/I_G value is lower than that obtained for the other films grown at ~450 and ~300 °C, while the sharpness of the peaks and the low Γ_G/q value indicate that considerable graphitization occurred in this film. Following this, the relation (3) was used to estimate L_a for this film. The cluster diameter L_a as a function of the N atomic ratio for different temperatures is presented in Fig. 2(e). One can observe that at RT, L_a increases with N incorporation. For 150 and 300 °C, L_a is higher than that obtained at RT and does not depend on the N content while at ~450 °C, N incorporation prevents the extension of graphene planes. The last observation indicates that N incorporated into the C matrix during IBS enters into bonding configurations that prevent the extension of the graphene planes. According to this, a high quantity of terminating pyridinelike or nitrilelike configurations could be expected, which is in agreement with XANES observations.[31]

The above analysis indicates that N plays a double role creating ordering or disorder depending on the growth temperature. At RT, an increasing N content in the films induces a decrease in the bond length and angle distortion (see also Refs. 16, 42, and 43). This is related to 2D sp^2 ordering and aromatic clustering resulting in higher L_a. In this regime, N incorporation is equivalent to an increase in temperature. When the films are grown above RT, L_a increases compared to the films grown at RT. However, L_a is nearly independent of both N content and substrate temperature in the 150–300 °C range. At 450 °C, N incorporation in the C network results in a sharp drop in L_a yielding the L_a values similar to that obtained at 150–300 °C. The following N incorporation does not result in any significant change of L_a. The fact that L_a decreases with low N addition indicates that some part of N is positioned at cluster edges and suppresses the temperature-induced cluster growth. This is probably due to the formation of pyridinelike sp^2 or nitrilelike sp^1 bonds. L_a becomes relatively low (~13–15 Å), so that a relatively large part of the cluster atoms is assumed to stay at the edges rather than inside the clusters. This means that a low fraction of N atoms in the terminating configurations can inhibit the cluster growth. However, the drop in L_a with N incorporation at ~450 °C is accompanied by a significant change in Γ_G/q. This may indicate that N substitutes C in sixfold rings, thus introducing high disorder inside the clusters. Additional N incorporation does not change Γ_G/q significantly. This indicates that the following N addition does not change the disorder inside the cluster, thus it can again be deduced that N is accumulating on the perimeter of the aromatic clusters. This corresponds to XANES observations of IBS CN_x films where N was found in the onefold, twofold, and threefold bonding configurations.[31]

Raman spectra of carbon nitride films grown with different N incorporation routes

When N is incorporated from the assisting ion beam/plasma in addition to N coming from the sputtered graphite target (DIBD and MS CN_x films), the Raman spectra of the films do not show appreciable differences from those of the CN_x films deposited at similar conditions but without ion assistance [see Fig. 1(b) for DIBD film and Fig. 1(c) for MS films]. In addition, the DIBD grown CN_x films show a similar degree of sixfold ring clustering and ordering as the CN_x films grown by IBS CN_x at similar temperature (see Table II). However, bond-angle distortion is considerably higher. This indicates that additional low-energy N ion bombardment does not interrupt significantly the cluster growth, while resulting in an almost double amount of incorporated N. This is compatible only if N atoms substitute C atoms in the graphitelike configurations, which is in agreement with

XANES observations.[31] On the other hand, MS grown CN_x films have high Γ_G and Γ_G/q values (~190–220 and ~80–105 cm^{-1}, respectively) combined with high L_a values (~15–16 Å), higher than those obtained in CN_x films grown by IBS or DIBD. This indicates that N incorporation from both sources—target and low-energy ions—does not hinder the growth of graphene planes while it introduces high disorder in sixfold ring structures. In addition, for films grown by MS, I_D/I_G ratios are very close and temperature-independent (~1.3, respectively). On the other hand, CN_x films grown by MS at 450 °C have considerably lower Γ_G and Γ_G/q values in comparison to those of the CN_x films grown by MS at 150 and 300 °C.

On the other hand, Raman spectra of the evaporated and IBAE grown films [Fig. 1(d)] present considerably sharper features indicating a higher degree of ordering in comparison to films grown by IBS, DIBD, and MS. For the *a*-C film evaporated at RT, the *D* peak can be clearly seen which is due to the deposition of the mixture of ablated clusters and evaporated atoms (see also Ref. 44). Similar Raman spectra were observed in C films grown by supersonic cluster deposition.[45] This is in contrast to *a*-C film grown by IBS at RT, where no visible contribution of the *D* peak could be observed. Low-energy (~60 eV) N ion assistance at RT results in lower intensity of the *D* peak, while an increase in temperature results in an increase of the contribution of the *D* peak. Raman spectra of the CN_x films grown by IBAE at 300 °C with different assisting ion current densities do not represent significant visible differences in comparison to those of the CN_x films grown at RT-480 °C [see Fig. 1(d)]. Similar tendencies have been observed for the spectra obtained at the same temperature for different current densities of assisting ion beam (not shown here).

In contrast, from the analysis of the evaporated at RT *a*-C and IBAE grown CN_x films, it follows that changing the assisting N ion flux for the given evaporation rate does not change *G* peak position, Γ_G or Γ_G/q (see Table II). As the IBAE growth is due to the deposition of preformed C clusters and atoms, it indicates that incoming energetic N ions do not affect significantly the cluster core, but accumulate on the cluster edges in terminating configuration or react with atomic C. In this case bonding strength, bond length, angle, and sixfold ordering are predetermined from incoming clusters. The dominance of terminating configurations is confirmed by XANES observations.[18] Besides, the I_D/I_G (correspondingly L_a) value of the CN_x film grown at 300 °C with the lowest assisting ion flux of 40 $\mu A\,cm^{-2}$ is higher than that of evaporated C film at RT, however it decreases when the assisting N ion flux increases up to 71 $\mu A\,cm^{-2}$. A further increase in assisting N ion flux does not change any parameter of the Raman spectra. For a given assisting N ion flux, the substrate temperature does not have any considerable influence except one film grown at RT. The *G* peak position and I_D/I_G is lower in comparison with the CN_x films grown at higher temperatures, while Γ_G is higher. This indicates that temperature-enhanced cluster growth, probably from the edges of already preformed clusters, is hindered by ion bombardment. These results shows that aromatic clustering during IBAE growth is a result of two concurrent processes—temperature and ion bombardment—which act in opposite directions. However, despite the fact that ion bombardment hinders efficiently the cluster growth, the sixfold ordering inside the clusters remains relatively high. Except for the CN_x film deposited with the lowest assisting N ion flux, I_D/I_G (correspondingly L_a) and Γ_G/q are relatively low (~0.8 and ~65 cm^{-1}, respectively) in comparison to those of IBS, DIBD, and MS grown CN_x with similar N contents (1.1–1.3 and ~80–100 cm^{-1}, respectively).

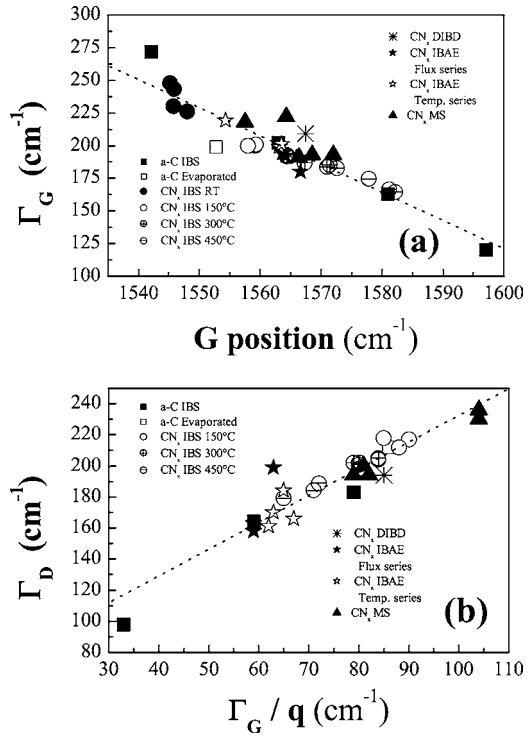

FIG. 3. Γ_G vs *G* peak position (a) and Γ_D vs Γ_G/q (b). Dashed lines represent linear fits.

Correlation between Raman fitting parameters

Figure 3(a) presents Γ_G as a function of the position of the *G* peak position for all the films produced for this study. A fairly good universal linear dependence is found, similar to that observed in *a*-C and *a*-C:H films in the same wavenumber region.[46] This is in agreement with a delocalized character of this vibration mode, and it reflects the fact that the bond strength is proportional to the bond length and angle distortion, but less to the origin of the distortions (defects, compositional changes). A similar linear dependence can also be seen for Γ_D as a function of Γ_G/q [Fig. 3(b)]. These linear relations permit us to reduce the number of independent parameters for further discussion. It follows that there remain only three independent parameters characterizing the *G* and *D* peaks: Γ_G (or *G* peak position), Γ_G/q (or Γ_D), and I_D/I_G.

Role of N incorporation and film structure on the clustering of sp^2 arrangements

The sixfold clustering in the C-N system is strongly affected by atomic mobility, damage (atomic displacements,

bond breaking) rate, and a chemical bond configuration of N in the C network. Without N incorporation, the sp^2 C network tends to cluster into 2D aromatic clusters, while an increase in atomic mobility results in the extension of the graphene planes, ordering inside the planes, and 3D graphitization[25,37,40,44] [see, for example, Figs. 2(c) and 2(e)]. However, when damage is introduced in near surface layers, the clustering rate is determined by an interplay of the damage rate and the temperature-enhanced clustering rate. When the damage is produced during film growth, another important parameter becomes the film growth rate.[47] The near surface displacements can only relax by the diffusion toward the surface, if the surface boundary velocity due to the film growth is smaller than the averaged velocity of the diffusing atoms.[47]

However, N incorporation into a C network significantly affects the aromatic clustering kinetics. First, N enhances the ordering process in a highly disordered C network[16] [see also Fig. 2(e)]. Secondly, N incorporation into the C network changes to some extent the bonding length between atoms comparing to the pure C network. Thirdly, N incorporation into the aromatic clusters induces warping[48] or favors the formation of the ring structures with an odd member of atoms per ring.[12,20] In addition, N incorporation favors cross-linking between adjacent planes.[12,21,22] And finally, some of the N bonding configurations, like pyridinelike or nitrilelike ones, act as the terminating configurations and hinder the cluster growth.[18,19,49–52] The dominance of each of these mechanisms depends on the way N is introduced into the C network, i.e., on the CN_x synthesis process.

Despite the comparable N contents observed in all CN_x films (see Table I), the comparison of the results from Raman analysis clearly shows significant differences in the degree of ordering and clustering for the CN_x films obtained by the different methods. When N is incorporated in the form of low-energy ions during the deposition of C clusters and atoms, the resulting CN_x films exhibit a high degree of bond length and angle distortion (represented by Γ_G), relatively high sixfold ring ordering (represented by Γ_G/q), and low cluster diameter (see Table II). On the other hand, when N originates from both sources—target and assisting plasma/beam (MS and DIBD)—the obtained C-N atomic arrangements can be characterized by a high degree of bond length and angle distortion, a high degree of disorder in sixfold clusters, and relatively large cluster sizes. When the sole N source is the sputtered nitrided graphite target, the grown CN_x films represent an intermediate case in terms of the aromatic cluster ordering and cluster size. The sixfold ring ordering of CN_x films deposited at lower temperatures is then close to that of the second type of films (MS and DIBD), while at higher temperatures it approaches that of the first type of CN_x films (IBAE). The bond length and angle distortion are comparable to that of the other CN_x film types only for the lower growth temperatures, while the increase in growth temperature results in lower Γ_G values. These observations correlate with previous transmission electron microscopy (TEM) and XANES results: MS grown CN_x exhibit FL microstructure with extended, curved, and interlinked graphene sheets and N occupying preferentially graphitelike sites[19,33]; IBAE grown CN_x are amorphous with N occupying

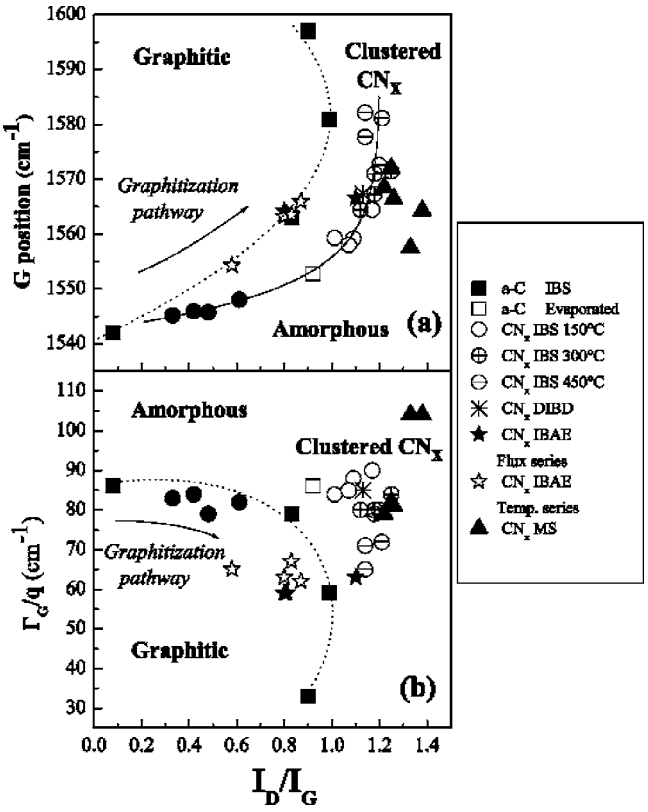

FIG. 4. G peak position (a) and coupling parameter Γ_G/q (b) vs I_D/I_G. Lines are guiding the eye only.

terminating low coordination number sites[18]; IBS CN_x present an intermediate case.[31,34] In addition, it can be concluded that promotion of N in the graphitelike environment results in a decrease of graphitic sixfold ordering (increase in Γ_G/q). Thus in relation to the film microstructure, only two parameters—Γ_G/q and I_D/I_G—are of interest: the latter reflects the average cluster size, while the former reflects the degree of sixfold ring ordering. Γ_G/q may be related to the average defect state and cross-linking of graphene sheets. As it can be seen from C films (Tables I and II), higher film densities correspond to higher Γ_G/q values. However, for CN_x the films' mass density increases with the degree of cross-linking, but decreases when the concentration of terminating CN configurations increases. Thus Γ_G/q may give valuable information about the cross-linking in CN_x films even when the density of the films does not reflect it directly (for example, for IBS grown CN_x at RT, the density decreases with N incorporation while Γ_G/q remains practically constant).

Graphitization pathways in carbon and carbon nitride films

For C films, an increase of temperature leads to graphitization, i.e., a decrease in local bond length and angle distortion Γ_G (increase in G peak position) and an increase in the sixfold ring ordering degree (decrease in Γ_G/q or Γ_D). However, N incorporation will perturb this graphitization pathway. Figure 4 presents the position and Γ_G/q of the G peak as a function of I_D/I_G. Figure 4(a) reflects changes in bond-

ing strength as a function of aromatic cluster size, while Fig. 4(b) reflects the aromatic ordering as a function of cluster size. The G peak position (Γ_G/q) versus I_D/I_G plot can be divided into three regions—amorphous, clustered, and graphitic. The graphitization pathway of any type of C films, will pass through all these stages. Following the graphitization pathway of IBS grown C films, it can be seen that the position of the G peak (Γ_G/q) increases (decreases) with I_D/I_G, reaches a maximum value of I_D/I_G, and continues to increase (decrease) when I_D/I_G decreases. This is consistent with the I_D/I_G dependence on the cluster size L_a (Ref. 23) [see Eqs. (3) and (4)]. The maximum value of I_D/I_G is $\sim$1.0 (also observed during annealing of ion implanted glassy carbon[41]), while according to Ref. 23 this maximum value is 2.2. This might be due to several reasons. The rough temperature steps ($\sim$150 °C) may not permit us to see larger values in the region 150–450 °C where this graphitization starts. Alternatively, the low-density values of the films obtained at 300 and 450 °C indicate porous structure, while Raman spectra show a relatively high degree of ordering. This may indicate a low nucleation rate and a high growth rate of graphitic clusters, higher grains shadowing smaller grains.[53] Relatively large graphitic clusters (several tens of nm) embedded in an amorphous matrix were observed by TEM in IBS a-C films grown at 450 °C.[54] Both large and small clusters result in a low I_D/I_G ratio. Thus scarce nucleation events during IBS growth may be followed by fast growth, resulting in the given graphitization pathway presumed above.

Carbon nitride films prepared by IBS follow another "graphitization pathway" shifted toward larger I_D/I_G values. In contrast to C films, higher temperatures do not decrease I_D/I_G. As it will be discussed below, the films experience a high amount of displacements during IBS growth, which hinder aromatic clustering. Nitrogen addition thus "softens" the damage produced by the incoming particles. In addition, the evaporated C film falls onto the CN_x "graphitization" pathway, but not on that of IBS grown C films, which is in agreement with the fact that the damage is absent during C evaporation, and that the flux of film-forming species consists of already preformed clusters. Moreover, once ion bombardment assists the growth of evaporated films, their pathway starts to follow that of a-C grown by IBS. The N ion to C atom ratio determines whether this pathway is close to the pathway of CN_x or C films grown by IBS. In addition, the data points of clustered CN_x films are concentrated in a small region of wave numbers (1560–1580 cm^{-1}) and I_D/I_G values (1.0–1.4). The latter observation indicates that N incorporation tends to reduce the effects of other factors, such as temperature or ion bombardment, and independently of growth conditions leads the system into the state with similar medium-range order [see also Figs. 2(a), 2(c), and 2(d)].

On the other hand, the sixfold ordering in IBS C films increases with the cluster size, which is expected during graphitization [Fig. 3(b)]. At the same time, it can be seen that IBS CN_x grown at RT follows the graphitization pathway of IBS C films. This indicates that progressive N incorporation into C at RT is equivalent to the temperature increase. N incorporation at higher temperatures shifts CN_x films out of the graphitization pathway of IBS C films, which reflects the fact that N reduces sixfold ordering in the clusters. Some ordering can be achieved by increasing the temperature, but in a limited manner. Evaporated C film exhibits similar graphitic ordering as IBS films accompanied with high average cluster size. However, ion bombardment during evaporation induces significant sixfold ordering, while increasing the N ion flux shifts the graphitization pathway toward lower I_D/I_G values.

Influence of low-energy ion bombardment and film growth rate on the clustering of sp^2 arrangements

The influence of the assisting ion bombardment is manifold. First of all, in reactive mode it introduces additional material. This can be seen in Table I, where N concentrations of 15–25 at. % can be obtained when N is delivered only by the assisting beam. This is also reflected by the N concentration of DIBD film, which is almost twice than that obtained without assisting N ion bombardment. On the other hand, during IBAE growth, the increase in N ion flux does not increase the N concentration, but results in a higher material loss (see Table I). This is related to the fact that a low-energy assisting ion bombardment activates or enhances surface processes. Molecular-dynamics simulations show that surface processes dominate when the energy of impinging atoms is $<$30 eV, while subsurface processes govern the structure formation for higher energies.[55] Consequently, hyperthermal atoms in the range up to $\sim$20 eV (Refs. 29 and 30) originating from the target due to sputtering mainly increase the mobility of the surface atoms,[30] which may result in enhanced aromatic clustering. Nevertheless, the very low intensity of the D peak in the Raman spectrum for the IBS a-C film grown at RT is observed. However, the elevated density (2.7 g cm^{-3}) of this film indicates that the structure is closely packed, thus a high degree of surface displacements due to incoming and backscattered particles might hinder the clustering of the sp^2 phase and densify the material (see also Ref. 56). Thus sixfold clustering during the C film growth, which is accompanied by a decrease of density with energetic particles, has to be related to the subsurface diffusion of C atoms, which becomes effective at higher temperature,[57,58] which in turn depends on the growth rate.[47] Thus the film growth may be considered as an interplay between incoming particle-induced displacements and temperature-induced relaxation. This also applies to the growth of CN_x films using energetic species in the temperature region of the present study
(RT-450 °C). It can be expected that sputtered preformed radicals have lower energy than the atomic species, or at least lower energy per atom. Following this, the incoming radicals may introduce less damage as energetic N or C atoms. As the N content in the sputtering beam or plasma increases, the ratio between radical and atomic growth species increases due to a higher probability of chemical reactions on the target surface, thus increasing the number of low-energy particles arriving at the surface of the growing film. Following this, a lower degree of damage may be expected for higher N_2 contents in the sputtering beam. Apart

from the N capability to favor aromatic clustering of the sp^2 phase,[16] a lower degree of damage from the incoming particles may also partially explain the higher degree of clustering for higher N content in IBS films grown at RT [see Fig. 2(e)].

On the other hand, even if the energy of a particle arriving at the film surface is insufficient to induce a displacement of surface atoms, also preexisting bonds between them may be splitted,[55] thus inducing chemical reactions that may also involve the incoming particle.[59] The energy threshold for bond breaking in the C-C system is of the order of several eV,[60] while the displacement energy is of the order of ~40 eV for graphite and diamond.[61,62] Similar bond breaking and displacement energies can be expected for the C-N system. Thus, there is a much larger probability for a bond-breaking event than for a displacement event. Therefore, it can be expected that a large amount of bonds are broken on the surface under the impingment of particles originating from the target due to sputtering, as well as from energetic ions. A majority of preformed C_xN_y $(x,y \leqslant 2)$ radicals coming from the sputtered target[32] can be expected to be affected by bombardment of energetic target species and from the assisting plasma/ion beam, making them available for chemical reactions, so that new atomic configurations can be formed under the influence of atomic mobility and ion bombardment. In the range of ion energies and fluxes used in this study, the supplementary moderate ion bombardment does not hinder the aromatic clustering during DIBD and MS. Moreover, in the case of MS sputtering, it even favors the cluster growth. It can be related to the fact that different atomic configurations have different damage thresholds.[63] Carbon and nitrogen atoms tend to form different concurrent atomic arrangements, which are allowed at a given temperature. However, only preferential formation of the phase with higher damage threshold takes place. According to this, moderate ion bombardment then favors the growth of the graphene sheets and N removal from terminating configurations, or N incorporation into graphite substitutional configurations through the ion-induced bond breaking and following reactions.

This mechanism may also partially explain the formation of the texture with standing graphitic basal planes during MS growth of FL-CN_x films.[49] As compressive stress cannot explain this phenomenon,[64] this may be due to the highest damage threshold of this atomic configuration. To a lower degree this texture is also observed in IBS films,[34] which are also submitted to bombardment with hyperthermal particles coming from the target. However, if the degree of ion bombardment is high enough, then formation of any ordered atomic configuration may be stopped. This may explain the complete amorphization of the MS CN_x films when the energy of the assisting ion bombardment increases from ~25 to ~40 eV for a pure N_2 atmosphere, while it still retains a high degree of clustering in the N_2/Ar mixtures.[33] This can be related to the mass difference of Ar and N ions. In the case of N ion irradiation, a higher fraction of the incoming ion energy can be transferred to surface C or N atoms due to close mass match.

In addition, it can be expected that the displacement or bond-breaking threshold is lower for $C \equiv N$ groups than for sp^2 C and N atoms inside or on the edges of aromatic clusters, because they are attached to the CN skeleton only by a single σ bond. For low ion energies (~25–40 eV), these groups may be preferentially removed, thus promoting incorporation of C and N atoms in more stable pyridinelike or graphitelike configurations. This may explain the high degree of clustering in MS films, where the removal of $C \equiv N$ groups may be expected in this range of ion energies, while the CN skeleton damage is still relatively low. For the DIBD film, which was prepared under N ion assistance at 100 eV, a high degree of ion-produced damage can be expected due to relatively high ion energy. However, this film exhibits a large in-plane disorder combined with a relatively high cluster size and a high N atomic ratio. This indicates a high degree of N incorporation in the graphitelike configuration, which is in agreement with XANES observations.[31] Apparently, the N ion bombardment hinders the formation of terminating configurations. This is in contradiction with the results concerning IBAE (this study) and MS (see Ref. 33) where the N energies above 40 eV led to the amorphization of CN_x.

This inconsistency may be related to thermal relaxation processes. The characteristic time of relaxation has to be compared to the characteristic time of atomic diffusion. During film growth, the latter is determined by the arrival rate of adsorbed species, i.e., the characteristic time during which an atom can move on the surface before becoming covered by further incoming species, and the displacement rate. During IBAE growth, the C arrival rate is very high (one order of magnitude higher than that during IBS). Assisting N ion bombardment even reduces the characteristic free migration time due to ion-induced displacements. On the other hand, the free migration time during IBS is significantly higher due to the low arrival rate of film-forming species, thus the damage introduced by incoming particles can be significantly reduced by thermal relaxation. It was observed that annealing of CN_x films leads to N incorporation into the graphitelike configurations.[66–68] Thus, when the relaxation rate is higher than the damage rate, it can be expected that N is preferentially integrated into graphitelike configurations. On the other hand, at ion energies below 40 eV most of the energy is deposited within the surface layer, while for higher energies deep displacements occur which can cause rearrangements of the CN network.[55] These bulk displacements may initiate some processes that favor N incorporation into the graphitelike configurations, while the energy being available for surface bond breaking may still result in the preferential removal of $C \equiv N$ groups.

Carbon nitride growth mechanisms during simultaneous deposition of carbon clusters and hyperthermal N ion irradiation

Different mechanisms appear when films are grown from a mixture of preexisting C clusters and atoms. Without N incorporation, an increase in growth temperature results in cluster growth and ordering.[44] This may be expected as incorporated atomic species can easily diffuse and accumulate on the edges of the preformed clusters. Nitrogen incorporation can hinder this process if N comes only in the form of

energetic ions. This may be related to the displacements of C atoms in the immediate vicinity of the N ion impact, thus lowering the number of C atoms available to react with the N ion. As a result, N is incorporated in low coordination number sites, which correlates with the Raman analysis results of this study (low Γ/q values for IBAE films) and XANES observations[18] (N preferentially in terminating configurations). This does not affect the ordering inside the clusters, while it effectively stops cluster growth, or even reduces the preexisting cluster size due to extensive bombardment (see Table II). This may explain the increase in sixfold ordering at RT, when C evaporation is additionally assisted with N ion bombardment: N ions react with C atoms forming volatile molecules, thus C atomic species do not participate in the C network, which results in more ordered structure as observed by Raman spectroscopy. The changes in film topology due to ion bombardment (probable formation of linear N terminated structures) can be investigated using dispersive Raman spectroscopy,[16] and new measurements using different excitations wavelengths are planned for the future.

Besides, for IBAE the incorporation rate strongly depends on the deposition parameters: it decreases by a factor of ~3 when the assisting ion flux increases for a fixed temperature by a factor of 2, while for a fixed ion flux it decreases by a factor of 1.4 when substrate temperature increases from RT to 450 °C. This decrease in incorporation rate at constant N/C ratio indicates that (i) an excess in N ion to atom ratio results in a loss of film-forming material (C and N) and (ii) C and N losses are correlated. This can be explained by ion-enhanced/induced formation of volatile CN compounds[53,69–73] via bond splitting and following chemical reactions. Bond splitting also explains the CN_x film amorphization during MS growth for higher ion energies and higher N_2 fraction in the gas.[33] It also explains a complete resputtering of the growing film even at lower ion energies (~25 eV) when N ion flux increases.[65]

In addition, an increase in N ion flux results not only in a decrease of incorporation rate, but also in a significant decrease of film mass density (see Table I). This may be related to the desorption of volatile CN compounds. When the N ion to C ratio is relatively low, these volatile species may be covered by incoming C atoms. Despite the fact that these compounds may diffuse toward the surface,[74] the high adsorption of C atoms traps these compounds inside the films. However, when the growth rate is lower, these volatile compounds may reach the surface more easily and may desorb, resulting in more and more porous material. Besides, for IBAE CN_x, the N atomic ratios are ~15 and ~23 at. % for the series of the samples grown to test the influence of assisting ion flux and temperature, respectively, and this does not depend either on temperature or on ion flux. The main difference between two series was the evaporation rate, which was higher by a factor of 2 for the series used to test the temperature influence. The same argument used to explain the density dependence on the ion bombardment can also explain the higher N concentration in the IBAE CN_x films grown with higher evaporation rate: volatile CN species remain trapped by incoming C atoms and clusters, thus resulting in higher N atomic ratio. This mechanism is in contrast to the observations that the N content increases when decreasing the film growth rate for the films obtained using atomic N flux assisted pulsed laser ablation.[75] This was attributed to the higher time the surface is exposed to atomic N flux, which increases the probability of N to react with surface atoms. This shows that different mechanisms are responsible for N incorporation using N in the form of energetic ions or atoms.

From the latter discussion, it follows that moderate N ion bombardment may favor the formation of a FL microstructure during the growth from preformed clusters with a certain degree of curvature (produced by electron beam evaporation, laser ablation, or cathodic arc) by preventing their graphitization due to accumulation on the cluster perimeter while selectively etching C atoms. Extensive ion bombardment reduces the cluster size, which results in the amorphous appearance observed by TEM.[18]

CONCLUSIONS

Sixfold ring clustering in sp^2-dominated C and CN_x thin films was investigated by Raman spectroscopy as a function of growth conditions (N incorporation routes, substrate temperature) and microstructure (amorphous, fullerenelike, nanographitic). For this purpose, C and CN_x films were grown using four different deposition methods, each of them involving different C sources (atoms and/or clusters) and N sources (mono- and multi-atomic species originating from the target, energetic ions originating from assisting ion beam/plasma). The Raman spectra in the wave-number number region of 1000–2000 cm^{-1} were analyzed by a combination of Lorentz-BWF functions for G and D peaks.

Independently of the film composition or growth method, it was found that G peak position (representing the bond strength) and width Γ_G (representing bond length and angle distortion) are interdependent. In addition, it was found that the G peak coupling parameter Γ_G/q and D peak width Γ_D—parameters of two different peaks, representing different vibration modes—are also interdependent and reflect the fact that both of them represent sixfold ring ordering. These linear relations significantly reduce the number of parameters that characterize the Raman spectra, while the latter relation permits us to extract some information about aromatic ordering in sp^2 phase when it cannot be directly accessed due to the low intensity of the D peak, which is directly related to the vibrations of sixfold rings. Besides, the latter parameters can be related to the degree of cross-linking in the sp^2-dominated films and describe the 3D connectivity of C and CN_x networks.

In the case of C films, the atomic structure evolves from a disordered network to nanocrystalline planar graphitic configurations, with a progressive promotion and ordering of sixfold rings clusters. When N is incorporated into a C network, a double role of N on sixfold ring clustering was identified which results in two different CN_x growth regimes: at low temperatures (<150 °C), the increase in N content in the films reduces bond length and angle distortion, increases cluster size, and decreases film mass density, while at higher temperatures (>150 °C) it introduces sixfold ring disorder and increases materials density. Generally, N incorporation

tends to reduce the effects of other factors, such as temperature or ion bombardment, and independently of growth conditions it tends to lead the CN system into the states with similar middle-range order.

The combination of Γ_G/q and I_D/I_G of the visible Raman spectra appears to a be powerful analysis tool for different types of CN_x, from which information not only about middle-range order but also about microstructure and even local bonding configuration can be indirectly deduced. Despite comparable N atomic ratios (10–25 at. %) obtained using different C and N incorporation routes, the analysis of *G* and *D* peaks reveals that each type of microstructure results can be associated with a characteristic set of values of these parameters, as follows.

(i) Amorphous CN_x films can be characterized by a low I_D/I_G value, while Γ_G/q reflects in which regime N is incorporated: high Γ_G/q values reflects N inducing aromatic clustering in disordered solid, and low Γ_G/q values indicate about N accumulated on the preformed cluster edges, which effectively hinders the cluster growth but has little effect on the cluster interior;

(ii) Fullerenelike CN_x films can be characterized by high Γ_G/q and I_D/I_G values, indicating large cluster sizes with N-induced large degree of disorder in the sixfold ring structure;

(iii) Intermediate structures with a large variety of Γ_G/q and I_D/I_G values.

The influence of low-energy (25–100 eV) ion/atom bombardment is very complex depending on the type, flux, and energy of the ions. When N is supplied only in the form of low-energy ions, it acts as a N source. However, the increase in N ion flux results in the loss of film-forming material. Additionally, depending on the energy and flux, energetic particle bombardment directs the growing film into certain atomic configurations by preferential displacements and bond splitting of the arrangements with low damage threshold. However, when ion bombardment increases, it results in the suppression of any ordered atomic structure either by amorphization or complete resputtering of film-forming material.

While C is incorporated in atomic and cluster form simultaneously, energetic N ions are incorporated preferentially on the cluster perimeter, which hinders the formation of extended graphene sheets but does not affect the sixfold ring ordering inside the clusters. The arrival ratio of N ions and preformed C clusters may determine the average cluster size, whereas N accumulation may prevent the graphitization and ordering process, which preserves the degree of sixfold ring ordering in the preformed clusters.

ACKNOWLEDGMENTS

This work has been carried out inside the IHP-Network "Synthesis, structure and properties of new fullerene-like materials" and supported by the EU Contract No. HPRN-CT-2002-00209. In addition, we would like to thank J. Neidhardt for providing MS grown CN_x samples.

*Electronic address: g.abrasonis@fz-rossendorf.de

[1] J. Neidhardt, L. Hultman, E. Broitman, T. W. Scharf, and I. L. Singer, Diamond Relat. Mater. **13**, 1882 (2004).
[2] E. Broitman, N. Hellgren, K. Järrendahl, M. P. Johansson, S. Olafsson, G. Radnóczi, J. E. Sundgren, and L. Hultman, J. Appl. Phys. **89**, 1184 (2001).
[3] T. Katsuno, S. Nitta, H. Habuchi, V. Stolojan, and S. R. P. Silva, Appl. Phys. Lett. **85**, 2803 (2004).
[4] V. S. Veerasamy, J. Yuan, G. A. J. Amaratunga, W. I. Milne, K. W. R. Gilkes, M. Weiler, and L. M. Brown, Phys. Rev. B **48**, 17954 (1993).
[5] B. Kleinsorge, A. C. Ferrari, J. Robertson, and W. I. Milne, J. Appl. Phys. **88**, 1149 (2000).
[6] S. Waidmann, M. Knupfer, J. Fink, B. Kleinsorge, and J. Robertson, J. Appl. Phys. **89**, 3783 (2001).
[7] M. Friedrich, Th. Welzel, R. Rochotzki, H. Kupfer, and D. R. T. Zahn, Diamond Relat. Mater. **6**, 33 (1997).
[8] A. Laskarakis, S. Logothetidis, and M. Gioti, Phys. Rev. B **64**, 125419 (2001).
[9] D. Das, K. H. Chen, S. Chattopadhyay, and L. C. Chen, J. Appl. Phys. **91**, 4944 (2002).
[10] M. Gioti and S. Logothetidis, Diamond Relat. Mater. **12**, 957 (2003).
[11] A. Y. Liu and M. L. Cohen, Science **245**, 841 (1989).
[12] H. Sjöström, S. Stafström, M. Boman, and J.-E. Sundgren, Phys. Rev. Lett. **75**, 1336 (1995).
[13] H. Sjöström, L. Hultman, J.-E. Sundgren, S. V. Hainsworth, T. F. Page, and G. S. A. M. Theunissen, J. Vac. Sci. Technol. A **14**, 56 (1996).
[14] W. T. Zheng, H. Sjöström, I. Ivanov, K. Z. Xing, W. R. Salaneck, J. E. Greene, and J.-E. Sundgren, J. Vac. Sci. Technol. A **14**, 2696 (1996).
[15] Z. J. Zhang, S. Fan, and C. M. Lieber, Appl. Phys. Lett. **68**, 2639 (1996).
[16] A. C. Ferrari, S. E. Rodil, and J. Robertson, Phys. Rev. B **67**, 155306 (2003).
[17] S. E. Rodil, Recent Res. Dev. Appl. Phys. **6**, 391 (2003).
[18] R. Gago, J. Neidhardt, M. Vinnichenko, U. Kreissig, Zs. Czigány, A. Kolitsch, L. Hultman, and W. Möller, Thin Solid Films **483**, 89 (2005).
[19] R. Gago, I. Jiménez, J. Neidhardt, B. Abendroth, I. Caretti, L. Hultman, and W. Möller, Phys. Rev. B **71**, 125414 (2005).
[20] A. Ilie, O. Harel, N. M. Conway, T. Yagi, J. Robertson, and W. I. Milne, J. Appl. Phys. **87**, 789 (2000).
[21] L. Hultman, J. Neidhardt, N. Hellgren, H. Sjöström, and J.-E. Sundgren, MRS Bull. **28**, 194 (2003).
[22] I. Jiménez, R. Gago, J. M. Albella, and L. J. Terminello, Diamond Relat. Mater. **10**, 1170 (2001).
[23] A. C. Ferrari and J. Robertson, Phys. Rev. B **61**, 14095 (2000).
[24] B. S. Elman, M. Shayegan, M. S. Dresselhaus, H. Mazurek, and G. Dresselhaus, Phys. Rev. B **25**, 4142 (1982).
[25] R. O. Dillon, J. A. Woollam, and V. Katkanant, Phys. Rev. B **29**,

3482 (1984).
[26] D. G. McCulloch, S. Prawer, and A. Hoffman, Phys. Rev. B **50**, 5905 (1994).
[27] S. E. Rodil, A. C. Ferrari, J. Robertson, and J. Muhl, Thin Solid Films **420-421**, 122 (2002).
[28] S. M. Rossnagel, J. Vac. Sci. Technol. A **21**, S74 (2003).
[29] K. Meyer, I. K. Schuller, and C. M. Falco, J. Appl. Phys. **52**, 5803 (1981).
[30] K. H. Müller, Phys. Rev. B **35**, 7906 (1987).
[31] G. Abrasonis, R. Gago, I. Jiménez, U. Kreissig, A. Kolitsch, and W. Möller, J. Appl. Phys. **98**, 074907 (2005).
[32] J. Neidhardt, L. Hultman, B. Abendroth, R. Gago, and W. Möller, J. Appl. Phys. **94**, 7059 (2003).
[33] J. Neidhardt, Zs. Czigány, I. F. Brunell, and L. Hultman, J. Appl. Phys. **93**, 3002 (2003).
[34] R. Gago, G. Abrasonis, A. Mücklich, Zs. Czigány, G. Radnóczi, and W. Möller, Appl. Phys. Lett. **87**, 071901 (2005).
[35] G. Abrasonis, R. Gago, M. Vinnichenko, M. Beckers, and N. Schell (unpublished).
[36] C. Thomsen and S. Reich, Phys. Rev. Lett. **85**, 5214 (2000).
[37] D. G. McCulloch and S. Prawer, J. Appl. Phys. **78**, 3040 (1995).
[38] F. Tuinstra and J. L. Koenig, J. Chem. Phys. **53**, 1126 (1970).
[39] G. Fanchini, G. Messina, A. Paoletti, S. C. Ray, S. Santangelo, A. Tagliaferro, and A. Tucciarone, Surf. Coat. Technol. **151-152**, 257 (2002).
[40] N. H. Cho, D. K. Veirs, J. W. Ager III, M. D. Rubin, C. B. Hopper, and D. B. Bogy, J. Appl. Phys. **71**, 2243 (1992).
[41] S. Prawer, F. Ninio, and I. Blanchonette, J. Appl. Phys. **68**, 2361 (1990).
[42] B. Kleinsorge, A. C. Ferrari, J. Robertson, W. I. Milne, S. Waidmann, and S. Hearne, Diamond Relat. Mater. **9**, 64 (2000).
[43] S. E. Rodil, A. C. Ferrari, J. Robertson, and W. I. Milne, J. Appl. Phys. **89**, 5425 (2001).
[44] S. Schelz, T. Richmond, P. Kania, P. Oelhafen, and H.-J. Güntherodt, Surf. Sci. **359**, 227 (2001).
[45] P. Milani, A. Podesta, P. Piseri, E. Barborini, C. Lenardi, and C. Castelnovo, Diamond Relat. Mater. **10**, 240 (2001).
[46] M. A. Tamor and W. C. Vassell, J. Appl. Phys. **76**, 3823 (1994).
[47] J. Koskinen, J.-P. Hirvonen, and J. Keränen, J. Appl. Phys. **84**, 648 (1998).
[48] M. C. dos Santos and F. Alvarez, Phys. Rev. B **58**, 13918 (1998).
[49] N. Hellgren, J. Guo, C. Såthe, A. Agui, J. Nordgren, Y. Luo, H. Ågren, and J. E. Sungren, Appl. Phys. Lett. **79**, 4348 (2001).
[50] N. Hellgren, J. Guo, Y. Luo, C. Såthe, A. Agui, S. Kashtanov, J. Nordgren, H. Ågren, and J.-E. Sungren, Thin Solid Films **471**, 19 (2005).
[51] W. J. Gammon, G. L. Hoatson, B. C. Holloway, R. L. Vold, and A. C. Reilly, Phys. Rev. B **68**, 195401 (2003).
[52] J. C. Sanchez-Lopez, C. Donnet, F. Lefebvre, C. Fernandez-Ramos, and A. Fernandez, J. Appl. Phys. **90**, 675 (2001).
[53] N. Hellgren, M. P. Johansson, E. Broitman, P. Sandström, L. Hultman, and J.-E. Sundgren, Thin Solid Films **382**, 146 (2001).
[54] G. Abrasonis, R. Gago, and A. Mücklich (unpublished).
[55] S. Uhlmann, Th. Frauenheim, and Y. Lifshitz, Phys. Rev. Lett. **81**, 641 (1998).
[56] J. J. Cuomo, J. P. Doyle, J. Bruley, and J. C. Liu, Appl. Phys. Lett. **58**, 466 (1991).
[57] H.-J. Scheibe, P. Siemroth, B. Schöneich, A. Mucha, and G. Kluge, Diamond Relat. Mater. **1**, 98 (1992).
[58] S. Sattel, T. Giessen, H. Roth, M. Scheib, R. Samlenski, R. Brenn, H. Ehrhardt, and J. Robertson, Diamond Relat. Mater. **5**, 425 (1996).
[59] C. Hopf, A. von Keudell, and W. Jacob, J. Appl. Phys. **94**, 2373 (2003).
[60] E. Salonen, K. Nordlund, J. Keinonen, and C. H. Wu, Phys. Rev. B **63**, 195415 (2001).
[61] H. J. Steffen, D. Marton, and J. W. Rabalais, Phys. Rev. Lett. **68**, 1726 (1992).
[62] J. Koike, D. M. Parkin, and T. E. Mitchell, Appl. Phys. Lett. **60**, 1450 (1992).
[63] Y. Lifshitz, S. R. Kasi, and J. W. Rabalais, Phys. Rev. Lett. **62**, 1290 (1989).
[64] K. F. McCarty, J. Vac. Sci. Technol. A **17**, 2749 (1999).
[65] N. Hellgren, K. Macák, E. Broitman, M. P. Johansson, L. Hultman, and J.-E. Sundgren, J. Appl. Phys. **88**, 524 (2000).
[66] I. Jiménez, W. M. Tong, D. K. Shuh, B. C. Holloway, M. A. Kelly, P. Pianetta, L. J. Terminello, and F. J. Himpsel, Appl. Phys. Lett. **74**, 2620 (1999).
[67] I. Jiménez, R. Gago, J. M. Albella, and L. J. Terminello, Diamond Relat. Mater. **10**, 1170 (2001).
[68] N. Hellgren, N. Lin, E. Broitman, V. Serin, S. E. Grillo, R. Twesten, I. Petrov, C. Colliex, L. Hultman, and J. E. Sundgren, J. Mater. Res. **16**, 3188 (2001).
[69] S. S. Todorov, D. Marton, K. J. Boyd, A. H. Al-Bayati, and J. W. Rabalais, J. Vac. Sci. Technol. A **12**, 3192 (1994).
[70] P. Hammer and W. Gissler, Diamond Relat. Mater. **5**, 1152 (1996).
[71] N. A. Morrison, S. E. Rodil, J. Robertson, and W. I. Milne, J. Appl. Phys. **89**, 5754 (2001).
[72] P. Hammer and F. Alvarez, Thin Solid Films **398-399**, 116 (2001).
[73] W. Jacob, C. Hopf, and M. Schlüter, Appl. Phys. Lett. **86**, 204103 (2005).
[74] J. Roth and J. Bohdansky, Appl. Phys. Lett. **51**, 964 (1987).
[75] Z. J. Zhang, S. Fan, and C. M. Lieber, Appl. Phys. Lett. **66**, 3582 (1995).